

RESEARCH ARTICLE

Robust Model Predictive Control for nonlinear discrete-time systems using iterative time-varying constraint tightening

Daniel D. Leister¹ | Justin P. Koeln²

¹Mechanical Engineering Department, The University of Texas at Dallas, Texas, USA

²Mechanical Engineering Department, The University of Texas at Dallas, Texas, USA

Correspondence

Corresponding author Justin Koeln.
Email: justin.koeln@utdallas.edu

Funding Information

This research was supported by the Office of Naval Research. Award number: N00014-22-1-2247.

Abstract

Robust Model Predictive Control (MPC) for nonlinear systems is a problem that poses significant challenges as highlighted by the diversity of approaches proposed in the last decades. Often compromises with respect to computational load, conservatism, generality, or implementation complexity have to be made, and finding an approach that provides the right balance is still a challenge to the research community. This work provides a contribution by proposing a novel shrinking-horizon robust MPC formulation for nonlinear discrete-time systems. By explicitly accounting for how disturbances and linearization errors are propagated through the nonlinear dynamics, a constraint tightening-based formulation is obtained, with guarantees of robust constraint satisfaction. The proposed controller relies on iteratively solving a Nonlinear Program (NLP) to simultaneously optimize system operation and the required constraint tightening. Numerical experiments show the effectiveness of the proposed controller with three different choices of NLP solvers as well as significantly improved computational speed, better scalability, and generally reduced conservatism when compared to an existing technique from the literature.

KEYWORDS

Nonlinear Model Predictive Control (MPC), Robust MPC, Constrained systems, Successive linearization.

1 | INTRODUCTION

The ability of Model Predictive Control (MPC) to optimize system operation while adhering to state and actuator constraints is one of the main reasons for its widespread popularity. Although under certain conditions nominal MPC possesses some inherent robustness to external disturbances¹, many applications require stronger robustness guarantees. This motivated the development of robust MPC formulations, where the potential effect of external unknown disturbances is explicitly taken into account and robust constraint satisfaction can be guaranteed for all future time steps. For linear systems, many robust MPC approaches rely on modifying the optimization problem by tightening the state and input constraints such that, by ensuring that the nominal predicted state trajectory is restricted to a tighter set of constraints, the real disturbed trajectories are still within the original constraints² or within a “tube” contained in the original constraints³.

Multiple approaches have been proposed to adapt robust MPC strategies for the nonlinear case, typically by applying some form of constraint tightening^{4,5,6,7,8,9,10,11,12,13,14}, with few exceptions¹⁵. However, striking a practical balance between computational complexity, conservatism, and implementation complexity remains a challenge for nonlinear robust MPC. Part of the challenge comes from the fact that constraint tightening requires quantifying the effect of uncertainties based on system dynamics. Doing so for nonlinear systems is not trivial and often compromises have to be made. Morato et al¹⁰, for example, propose using the framework of Linear Differential Inclusion, which leverages many of the benefits of linearity while still capturing the nonlinear nature of the system, but note that this may yield conservative disturbance propagation sets. Köhler et al⁹ propose tightening the inequality constraints through the use of scalar variables that capture the “tube sizes”, computed based on level sets of Lyapunov functions. The approach though requires that the system be incrementally stabilizable. Mayne et al⁷ somewhat simplify the problem of finding tightened constraint sets by defining these sets as scaled-down versions of the original input and state constraint sets, although it is not clear how much conservatism this may introduce. Pin et al⁵ propose computing

the constraint tightening based on Lipschitz constants of the nonlinear dynamics function, which tend to produce conservative results^{10,9,12}. Separate control and prediction horizons are proposed to overcome this issue by applying constraint tightening and a terminal set constraint only within the shorter control horizon, thereby reducing the propagation of errors⁵. Doff-Sotta and Cannon¹² derive a Tube-MPC algorithm for difference-of-convex systems, a relatively general class of nonlinear systems. Their algorithm relies on the idea of iteratively solving a series of convex problems at each time step, where each problem solution generates a reference trajectory used to obtain a new linear system representation and a new linear feedback controller. However, their formulation does not consider external disturbances.

Constraint tightening-based robust Nonlinear MPC (NMPC) approaches commonly use a Linear Time-Varying (LTV) approximation of the nonlinear dynamics, obtained by linearizing about a reference trajectory, to facilitate the tightening of constraints. This naturally introduces the issue of having to bound linearization errors. Also, these formulations often use a linear feedback component in the control input, acting on the error between the nominal and the actual system trajectory. This provides the controller with the ability to limit the effect of disturbances and linearization errors on the nominal trajectories when predicting the future effect of disturbances. These approaches have the challenge of coping both with linearization errors *and* the effect of external disturbances. Leeman et al¹³ argue that the traditional approach of solving robust optimal control problems by optimizing a reference trajectory and designing a stabilizing feedback controller offline introduces conservatism. They propose lumping linearization, parameterization, and disturbance errors into sets that are parameterized by decision variables in the optimization problem. Similarly, the linear feedback gains are also part of the decision variables. This setup arguably removes complexity from offline design and reduces conservatism, with the potential drawback of increased complexity of the resulting optimization problem.

The controller proposed in this work shares similarities with some of the existing work in that i) LTV models obtained from reference trajectories form the basis of computing overapproximations of error sets^{11,12,13,14}, ii) an iterative procedure is used to optimize planned trajectories^{15,11,12,14}, iii) efficient set representations such as zonotopes and intervals are used to reduce computation times^{4,5}, and iv) a fallback control option is used when no adequate solution to the optimization problem can be found at certain time steps⁴. However, this work differs from the existing works in some key aspects. The linear feedback controller and the corresponding constraint tightening are recomputed *online and iteratively*, which is enabled by the use of efficient set representations and a practical approach to account for the effect of linearization errors and external disturbances. The constraint tightening approach used here is inspired by the method developed by Richards² for robust MPC for LTV systems, which differs from the traditional tube-based MPC formulation. With this strategy, the approach used in this work addresses the conservatism issue mentioned by Leeman et al¹³ without introducing additional complexity to the optimization problem. Note that, in the work of Kim et al¹⁴ and Messerer et al¹¹ the optimized trajectory, the gains of the linear feedback controller, and the constraint tightening are also computed iteratively in a similar fashion to the approach used in this work. However, both references make use of ellipsoids for the representation of error sets while this work uses zonotopes and intervals. Moreover, Kim et al¹⁴ rely on the estimation of local Lipschitz constants and the control gains are obtained from the solution to a Semidefinite Program (SDP), while Messerer et al¹¹ use a Ricatti recursion procedure to compute the control gains. Although their main algorithms share similarities with the proposed technique, the resulting formulations are considerably different. A recent work by Leeman et al¹⁶ combines benefits of System Level Synthesis (SLS)¹³ with the fast Ricatti recursion scheme¹¹ to derive a robust MPC for Linear Time-Varying systems with significant speed improvements compared to formulations based on off-the-shelf solvers. An extension to nonlinear systems is provided in the appendix of the referred work though no numerical examples are provided for the nonlinear case. Therefore, a comparison provided in Section 7 is restricted to the formulation from 13.

Therefore, the main contribution of this work lies in proposing a novel shrinking-horizon robust NMPC formulation for discrete-time systems that relies on iterative time-varying constraint tightening to obtain robust constraint satisfaction guarantees and the ability to run in real time with potentially suboptimal performance. The shrinking horizon formulation is motivated by applications where the controller is expected to operate for a fixed period of time and steady-state equilibria do not simultaneously satisfy input and state constraints, such as aircraft missions that consist entirely of transient operation¹⁷. Technical details for formulating an MPC controller with a shrinking horizon are provided by Koeln and Alleyne¹⁸.

The remainder of this paper is organized as follows. Section 2 defines the class of nonlinear dynamic systems considered and the control problem to be solved. Section 3 details the computation of error sets used for constraint tightening. Section 4 shows how constraint tightening based on a time-varying Linear Quadratic Regulator (LQR) can provide robust constraint satisfaction. Section 5 details the proposed controller formulation while Section 6 provides some considerations for practical implementation. Finally, Section 7 details results of using the proposed controller in simulations with a nonlinear system, including a performance comparison with one of the existing techniques in the literature.

1.1 | Notation

The letters i, k, l , and m , when used in the subscripts, are used for time step indexing in the discrete-time dynamics of the models and controllers. The set of integers in the interval $[k, k+i] \subset \mathbb{R}$ is denoted \mathbb{Z}_k^{k+i} . In the context of MPC predictions, a double-index notation is used such as in x_{k+il} , where the first subscript $k+i$ is the time step index of the predicted variable and the second subscript k is the time step index when such prediction is made. When all matrices have the same indexes, the shorthand notation $(A+BK)_{k+il}$ will be used to represent $(A_{k+il} + B_{k+il}K_{k+il})$. The variables n_x , n_u , and n_d represent the number of states, inputs, and disturbances in the dynamic models. Superscript r is used for variables of a *reference* trajectory used to obtain LTV models. The variable N refers to the final time step in the system operation. Bold capital letters such as \mathbf{X} represent a collection of vectors that refer to a trajectory in time. The variable $\mathbf{X}_k = \{x_{kl}, \dots, x_{k+N|k}\}$, with $x_{k+il} \in \mathbb{R}^{n_x}$, refers to a state trajectory, $\mathbf{U}_k = \{u_{kl}, \dots, u_{k+N-1|k}\}$, with $u_{k+il} \in \mathbb{R}^{n_u}$, to an input trajectory, and $\mathbf{D}_k = \{d_k, \dots, d_{k+N-1}\}$, with $d_{k+i} \in \mathbb{R}^{n_d}$, to a disturbance trajectory. The operation $\mathcal{A} \oplus \mathcal{B} = \{a+b \mid a \in \mathcal{A} \text{ and } b \in \mathcal{B}\}$ is the Minkowski sum and $\mathcal{A} \ominus \mathcal{B} = \{a \mid (a+b) \in \mathcal{A}, \forall b \in \mathcal{B}\}$ is the Pontryagin difference of sets \mathcal{A} and \mathcal{B} . The combined product of matrices M_i is represented with $\prod_i^k M_i$, where matrices with increasing indexes are *multiplied to the left*. The symbol I is used for the identity matrix of proper dimensions. The $\text{diag}(x)$ operator is used to represent a diagonal matrix whose diagonal elements are given by the elements of the vector x .

2 | DEFINITIONS AND PROBLEM STATEMENT

Consider a system that operates for a fixed time period with discrete-time nonlinear dynamics given by

$$x_{k+1} = f(x_k, u_k, d_k), \quad (1)$$

where the nonlinear mapping $f(\cdot)$ is twice continuously differentiable, $x_k \in \mathbb{R}^{n_x}$ represents the system states, $u_k \in \mathbb{R}^{n_u}$ the inputs, and $d_k \in \mathbb{R}^{n_d}$ the external disturbances. The system operation is considered to happen over $N \in \mathbb{Z}_+$ time steps such that $k \in \mathbb{Z}_0^N$.

Also, the system is subject to output constraints of the form

$$y_k = (C_k x_k + D_k u_k) \in \mathcal{Y}_k, \quad (2)$$

where C_k and D_k are suitably defined matrices such that the output constraint sets \mathcal{Y}_k represent input and state constraints of the system being controlled or any linear combination thereof. With $k \in \mathbb{Z}_0^N$, it is assumed that $D_N = 0$ in (2) such that $y_N \in \mathcal{Y}_N$ imposes a terminal constraint on x_N alone.

Assumption 1. Sets \mathcal{Y}_k are assumed to be compact and convex sets of suitable dimensions.

At any time step k , the total disturbance to the system can be split into a known component and an unknown component

$$d_k = d_k^r + \Delta d_k. \quad (3)$$

Here, d_k^r is the known part (i.e. the reference disturbance) and refers to the expected or predicted nominal disturbance trajectory. The term Δd_k is the unknown component.

Assumption 2. The disturbance deviation Δd_k is bounded, for all $k \in \mathbb{Z}_0^{N-1}$, by some known compact set \mathcal{D}_k centered at the origin.

The goal of this work is to derive a nonlinear shrinking-horizon robust MPC to control system (1) while providing robustness guarantees for any possible realization of disturbance trajectory \mathbf{D}_0 . Ultimately, the goal is to find a controller that optimizes system operation according to the optimization problem

Problem 1:

$$\min_{\mathbf{X}_0, \mathbf{U}_0} \ell(\mathbf{X}_0, \mathbf{U}_0), \quad (4a)$$

$$\text{s.t. } \forall k \in \mathbb{Z}_0^{N-1} \text{ and } \forall \Delta d_k \in \mathcal{D}_k,$$

$$x_{k+1} = f(x_k, u_k, d_k^r + \Delta d_k), \quad (4b)$$

$$y_k = C_k x_k + D_k u_k, \quad (4c)$$

$$y_k \in \mathcal{Y}_k, \quad y_N \in \mathcal{Y}_N, \quad (4d)$$

where $\ell(\mathbf{X}_0, \mathbf{U}_0)$ is some convex function of the state and input variables and x_0 is a known initial condition.

3 | COMPUTATION OF ERROR SETS

Since error sets play a key role in tightening constraints to achieve robustness, this section details how these sets can be computed based on bounds on linearization errors and disturbances. The error sets are obtained based on an assumed feedback behavior of the controller for future time steps as well as how the effects of linearization errors and disturbances are propagated through the linearized system dynamics.

3.1 | Linearized system model

Before deriving a linearized model of the system, a reference trajectory is defined as follows.

Definition 1 (Reference Trajectory). In the context of this work, a reference trajectory $\mathbf{Z}_k^r = \{z_k^r, \dots, z_{N-1}^r\}$, where $z_k^r = (x_k^r, u_k^r, d_k^r)$, is a trajectory around which the dynamics in (1) are linearized to obtain a LTV model of the system. Reference trajectories do not necessarily satisfy the dynamics in (1), unless otherwise stated.

Considering some reference trajectory \mathbf{Z}_k^r , the nonlinear system dynamics (1) can be rewritten using a Taylor expansion as follows

$$x_{k+1} = A_k x_k + B_k u_k + V_k d_k + c_k + \zeta(\xi_k), \quad (5)$$

where

$$A_k = \left. \frac{\partial f(x, u, d)}{\partial x} \right|_{(x_k^r, u_k^r, d_k^r)}, \quad (6a)$$

$$B_k = \left. \frac{\partial f(x, u, d)}{\partial u} \right|_{(x_k^r, u_k^r, d_k^r)}, \quad (6b)$$

$$V_k = \left. \frac{\partial f(x, u, d)}{\partial d} \right|_{(x_k^r, u_k^r, d_k^r)}, \quad (6c)$$

$$c_k = f(x_k^r, u_k^r, d_k^r) - A_k x_k^r - B_k u_k^r - V_k d_k^r, \quad (6d)$$

and $\zeta(\xi_k)$ is the Lagrange remainder (linearization error) of the Taylor expansion, with $\xi_k \in \mathcal{Z}_k^\xi = \{z_k^r + \alpha(z_k - z_k^r) | \alpha \in [0, 1]\}$.

A nominal LTV system representation is obtained when the linearization error is ignored and only reference disturbances are considered in (5)

$$\hat{x}_{k+1} = A_k \hat{x}_k + B_k \hat{u}_k + \hat{c}_k, \quad (7)$$

where

$$\hat{c}_k = f(x_k^r, u_k^r, d_k^r) - A_k x_k^r - B_k u_k^r.$$

3.2 | Derivation of error sets from linearized dynamics

The dynamics in (1) are said to represent the *nominal nonlinear dynamics* if the system evolution is considered when subject to a reference disturbance d_k^r and not the actual disturbance d_k . The second subscript here is applied to x_{k+ilk} to make clear that this is the time step when the error is being predicted. The error between the actual states and the nominal LTV state trajectory is defined as

$$e_{k+ilk} = x_{k+ilk} - \hat{x}_{k+ilk}. \quad (8)$$

In order to obtain upper bounds on this error, the controller is considered to take the form

$$u_{k+ilk} = \hat{u}_{k+ilk} + K_{k+ilk} e_{k+ilk}, \quad (9)$$

where, similar to the derivation by Richards², the linear feedback control matrices K_{k+ilk} are obtained from a time-varying finite-horizon LQR controller formulation as detailed in Appendix A.

Now note that for the current time step, when $i = 0$, $e_{kilk} = 0$ due to the fact that all state trajectories start from the current measured state, which is assumed to be known. In other words: $x_{kilk} = \hat{x}_{kilk}$. Therefore, starting from the next time step, where $e_{k+1lk} = x_{k+1lk} - \hat{x}_{k+1lk}$, and using (5) and (9) to propagate the error dynamics forward, it can be shown that

$$e_{k+ilk} = \sum_{l=0}^{i-1} \hat{V}_{k+l lk}^i \Delta d_{k+l} + \sum_{l=0}^{i-1} \hat{G}_{k+l lk}^i \zeta(\xi_{k+l lk}), \quad (10)$$

with

$$\begin{aligned} \hat{G}_{k+l lk}^i &= \begin{cases} \left(\prod_{m=l+1}^{i-1} (A + BK)_{k+m lk} \right), & \text{for } l \in \mathbb{Z}_0^{i-2}, \\ I, & \text{for } l = i-1, \end{cases} \\ \hat{V}_{k+l lk}^i &= \hat{G}_{k+l lk}^i V_{k+l lk}, \text{ for } l \in \mathbb{Z}_0^{i-1}. \end{aligned}$$

Using Assumption 2 and (10), the total error at each time step can be bound by

$$\mathcal{E}_{k+ilk} = \bigoplus_{l=0}^{i-1} \left(\hat{V}_{k+l lk}^i \mathcal{D}_{k+l} \oplus \hat{G}_{k+l lk}^i \mathcal{L}(\mathcal{Z}_{k+l lk}) \right), \quad (11)$$

where $\mathcal{Z}_{k+l lk}$ is such that $\mathcal{Z}_{k+l lk}^\xi \subseteq \mathcal{Z}_{k+l lk}$ and \mathcal{L} is a set operator that overapproximates the set of possible values of the Lagrange remainder $\zeta(\xi_{k+l lk})$ given $\mathcal{Z}_{k+l lk}$. There are multiple methods of implementing the \mathcal{L} operator to compute overapproximations for linearization errors¹⁹. The method used in this work is detailed in Section 6.2.

To obtain the sets $\mathcal{Z}_{k+l lk}$, consider the following definition for the elements of the set

$$z_{k+l lk} = z_{k+l lk}^r + \Delta z_{k+l lk},$$

with

$$\Delta z_{k+l lk} = z_{k+l lk} - z_{k+l lk}^r = \begin{bmatrix} x_{k+l lk} - x_{k+l lk}^r \\ u_{k+l lk} - u_{k+l lk}^r \\ d_{k+l} - d_{k+l}^r \end{bmatrix}.$$

Assumption 3. The open-loop control component in (9) is taken as the reference input trajectory, i.e., $\hat{u}_{k+ilk} = u_{k+ilk}^r$.

If Assumption 3 holds and considering that $\hat{x}_{k+l|k}$ is obtained from the LTV dynamics linearized around $x_{k+l|k}^r$ and both consider the nominal reference disturbance, then $\Delta z_{k+l|k}$ can be rewritten as

$$\Delta z_{k+l|k} = \begin{bmatrix} x_{k+l|k} - \hat{x}_{k+l|k} \\ u_{k+l|k} - \hat{u}_{k+l|k} \\ d_{k+l} - d_{k+l|k}^r \end{bmatrix}. \quad (12)$$

Now using (8) and (9), $\Delta z_{k+l|k}$ becomes

$$\Delta z_{k+l|k} = \begin{bmatrix} e_{k+l|k} \\ K_{k+l|k} e_{k+l|k} \\ \Delta d_{k+l} \end{bmatrix}.$$

Therefore, the sets $\mathcal{Z}_{k+l|k}$ can be written as

$$\mathcal{Z}_{k+l|k} = z_{k+l|k}^r \oplus (\mathcal{E}_{k+l|k} \times K_{k+l|k} \mathcal{E}_{k+l|k} \times \mathcal{D}_{k+l}). \quad (13)$$

From (11) and (13), it can be seen that the sets \mathcal{E} depend on the sets \mathcal{Z} computed for previous time steps while the sets $\mathcal{Z}_{k+l|k}$ depend on the corresponding $\mathcal{E}_{k+l|k}$ sets. Algorithm 1 summarizes the steps needed to compute these sets sequentially based on a reference trajectory.

Algorithm 1 Error Sets Computation

Require: $z_{k+l|k}^r$ for all $i \in \mathbb{Z}_0^{N-1}$

- 1: $\mathcal{E}_{k|k} = \mathbf{0}$ ▷ due to $e_{k|k} = 0$
 - 2: $\mathcal{Z}_{k|k} = z_{k|k}^r \oplus (\mathbf{0} \times \mathbf{0} \times \mathcal{D}_k)$ ▷ from (13)
 - 3: **for** $i = 1 \dots N-1$ **do**
 - 4: compute $\mathcal{E}_{k+i|k}$ using (11)
 - 5: compute $\mathcal{Z}_{k+i|k}$ using (13)
 - 6: **end for**
 - 7: compute $\mathcal{E}_{k+N|k}$ using (11)
 - 8: **return** $\mathcal{E}_{k+i|k}$ for all $i \in \mathbb{Z}_1^N$
-

4 | LQR-BASED CONSTRAINT TIGHTENING AND ROBUST CONSTRAINT SATISFACTION

With the method outlined in Algorithm 1 to compute error sets, this section demonstrates how the controller defined in (9) provides a suboptimal control law that robustly satisfies the system's output constraints, given a reference trajectory that satisfies certain conditions at time step $k = 0$.

4.1 | Preliminaries

Assumption 4. Given two sets \mathcal{A} and \mathcal{B} , if $\mathcal{A} \subseteq \mathcal{B}$ then $\mathcal{L}(\mathcal{A}) \subseteq \mathcal{L}(\mathcal{B})$, with \mathcal{L} the set operator defined in Section 3.

Proposition 1 (Morphological Opening Property²⁰). *Given compact and closed sets \mathcal{A} and \mathcal{B} containing the origin, then*

$$(\mathcal{A} \ominus \mathcal{B}) \oplus \mathcal{B} \subseteq \mathcal{A}. \quad (14)$$

Also, consider the tightened output constraint sets $\hat{\mathcal{Y}}_{k+i|k}$, which are related to the original output constraints such that

$$\hat{\mathcal{Y}}_{k+i|k} = \mathcal{Y}_{k+i} \ominus [(C_{k+i} + D_{k+i} K_{k+i|k}) \mathcal{E}_{k+i|k}]. \quad (15)$$

The tightened constraint sets $\hat{\mathcal{Y}}_{k+il|k}$ depend directly on $K_{k+il|k}$ and $\mathcal{E}_{k+il|k}$. These error sets $\mathcal{E}_{k+il|k}$, as seen in Section 3, also depend on the LQR gain matrices, namely on $K_{k+l|k}$ for all $l \in \mathbb{Z}_1^{i-1}$. However, these $K_{k+l|k}$ are obtained by linearization around the references $z_{k+l|k}^r$. Therefore, the tightened constraint sets $\hat{\mathcal{Y}}_{k+il|k}$ are directly related to the specific references $z_{k+il|k}^r$.

Definition 2 (Valid Reference Trajectory). At time step k , a reference trajectory $\mathbf{Z}_k^r = \{z_{k|k}^r, \dots, z_{N-1|k}^r\}$ is said to be *valid* if it satisfies the nonlinear dynamics (1) and the resulting outputs from (2) satisfy the corresponding tightened output constraint sets $\hat{\mathcal{Y}}_{k+il|k}$, $i \in \mathbb{Z}_0^{N-k}$, obtained using this reference trajectory.

4.2 | Robust constraint satisfaction

Now, the main result of this section can be stated as follows.

Theorem 1. For any time step $k \in \mathbb{Z}_0^{N-1}$, if disturbances are bounded according to Assumption 2, a valid reference trajectory \mathbf{Z}_k^r is known, and system (1) is controlled by the input (9) with $\hat{u}_{k+i|k} = u_{k+i|k}^r$ for all $i \in \mathbb{Z}_0^{N-k-1}$, then the actual system outputs y_{k+i} will satisfy the original output constraints \mathcal{Y}_{k+i} for all $i \in \mathbb{Z}_0^{N-k}$.

Proof. Consider the definition of the system output at time step $k+i$

$$y_{k+i} = C_{k+i}x_{k+i} + D_{k+i}u_{k+i}.$$

Substituting x_{k+i} and u_{k+i} using (8) and (9), one obtains

$$\begin{aligned} y_{k+i} &= C_{k+i}(\hat{x}_{k+i|k} + e_{k+i|k}) + D_{k+i}(\hat{u}_{k+i|k} + K_{k+i|k}e_{k+i|k}), \\ &= \hat{y}_{k+i|k} + (C + DK)_{k+i|k}e_{k+i|k}. \end{aligned}$$

Notice that, as $\hat{u}_{k+i|k} = u_{k+i|k}^r$, the nominal LTV state trajectory is equal to the state reference trajectory, i.e., $\hat{x}_{k+i|k} = x_{k+i|k}^r$, since there are no linearization errors on the reference trajectory. So, $\hat{y}_{k+i|k} = y_{k+i|k}^r$ and, from Definition 2, it results that $\hat{y}_{k+i|k} \in \hat{\mathcal{Y}}_{k+i|k}$. Therefore

$$y_{k+i} \in \hat{\mathcal{Y}}_{k+i|k} \oplus (C + DK)_{k+i|k}\mathcal{E}_{k+i|k}.$$

Using (15),

$$y_{k+i} \in \mathcal{Y}_{k+i} \ominus (C + DK)_{k+i|k}\mathcal{E}_{k+i|k} \oplus (C + DK)_{k+i|k}\mathcal{E}_{k+i|k}.$$

Applying the opening property from (14) results in $y_{k+i} \in \mathcal{Y}_{k+i}$ and the proof is complete. \square

This result shows that, if a valid reference trajectory can be found at time step $k = 0$, then applying the LQR-based control law given by (9) guarantees robust constraint satisfaction for all future time steps. This control strategy though is not necessarily optimal. The MPC controller proposed in Section 5 aims at achieving better performance while keeping the robustness guarantees from Theorem 1.

Remark 1. Note that, when deriving the LQR control gains $K_{k+i|k}$, no assumption is made with respect to the stabilizability of the underlying LTV system, originating from a reference trajectory satisfying the nonlinear dynamics. However, the LQR control in (9) acts to minimize deviations of the actual trajectory from the reference trajectory. Therefore, the less effective the LQR control is in minimizing these errors, the larger the error sets $\mathcal{E}_{k+i|k}$ and the smaller the tightened constraint sets $\hat{\mathcal{Y}}_{k+i|k}$. In the extreme case, the error sets may be so large that some of the tightened constraint sets become empty and no valid reference trajectory exists. This ultimately depends on the nonlinear dynamics of the specific system being considered and the weighting matrices of the LQR control design.

5 | PROPOSED ROBUST NMPC

This work proposes a novel shrinking-horizon nonlinear robust MPC with a fallback control component. The fallback control is used when no valid solution to the MPC optimization problem can be found within the controller's sampling time, while still guaranteeing robust constraint satisfaction. The proposed controller *iteratively* solves the optimization problem

Problem 2:

$$\min_{\mathbf{X}_k, \mathbf{U}_k} \ell(\mathbf{X}_k, \mathbf{U}_k), \quad (16a)$$

$$\text{s.t. } \forall i \in \mathbb{Z}_0^{N-k-1}$$

$$x_{k+i+1|k} = f(x_{k+i|k}, u_{k+i|k}, d_{k+i}^r), \quad (16b)$$

$$x_{k|k} = x_k, \quad (16c)$$

$$y_{k+i|k} = C_{k+i}x_{k+i|k} + D_{k+i}u_{k+i|k}, \quad (16d)$$

$$y_{k+i|k} \in \hat{\mathcal{Y}}_{k+i|k}, \quad y_{N|k} \in \hat{\mathcal{Y}}_{N|k}. \quad (16e)$$

Since d_{k+i}^r represents the known or expected disturbance values at each time step, (16b) refers to the *nominal* nonlinear dynamics of the system. Equation (16e) enforces constraining the nominal outputs to the tightened output constraint sets $\hat{\mathcal{Y}}_{k+i|k}$ as defined in (15). This implies that **Problem 2** is tied to a specific reference trajectory since the constraint tightening is obtained from a reference trajectory as noted in Section 4.1. This trajectory though is not necessarily a *valid* reference trajectory, as will become clear in the remainder of this section.

5.1 | Obtaining valid optimal reference trajectories

Given that the control strategy in (9) provides a robust control strategy that is suboptimal, the controller proposed in this work uses **Problem 2** to obtain an optimized and valid reference trajectory at each time step, as shown in Algorithm 2. The algorithm starts with a given initial reference trajectory and iteratively goes through the process of solving **Problem 2** to obtain a new reference trajectory, computing the LQR controller gains and tightened output constraints, and verifying whether the new reference trajectory is valid with respect to the tightened output constraints. The algorithm terminates either when a new optimized valid reference trajectory is found or the maximum number of iterations is exceeded, in which case it is considered to have failed to find such an optimized trajectory.

Also, within the scope of this work, no claims are made with respect to the convergence properties of the sequence of reference trajectories obtained in Algorithm 2 or its ability to return a new valid reference trajectory. The availability of a fallback control input is therefore essential to guarantee closed-loop robust constraint satisfaction of the proposed controller as detailed in Section 5.2.

5.2 | Main controller algorithm

Algorithm 3 summarizes the proposed controller formulation. Note that, since the Algorithm 2 may not converge to a valid solution within the maximum number of steps in Line 5, the controller needs to provide a fallback control input as shown in Line 11. On the other hand, if Algorithm 2 converges to a valid solution at some time step k_v , the obtained solution is used to update the reference trajectory \mathbf{Z}^r . This reference trajectory is stored, along with the corresponding LQR matrices, for use in future time steps to compute the fallback control input. At any time step, the proposed controller guarantees robust constraint satisfaction even if Algorithm 2 never again finds a valid solution, using the fallback option for the remaining time steps. The fallback option though provides a suboptimal control response, therefore it is desirable that the algorithm finds a valid solution in as many time steps as possible in order to obtain optimized control inputs.

Next, the robustness guarantees of the proposed controller are presented.

Assumption 5. At time step $k = 0$, an initial valid reference trajectory $\mathbf{Z}_0^r = (\mathbf{X}_0^r, \mathbf{U}_0^r, \mathbf{D}_0^r)$ is available.

Theorem 2. If Assumptions 5 and 2 hold true, then system (1), with control inputs given by Algorithm 3, robustly satisfies the original output constraints (2) at all time steps within the system operation, i.e., for $k \in \mathbb{Z}_0^N$.

Algorithm 2 Valid Reference Trajectory Optimization

Require: $u_0, x_0, \mathbf{X}_0^r, \mathbf{U}_0^r, \mathcal{D}_k, \mathcal{Y}_k$, maxIters $\triangleright \mathbf{U}_0^r$ and \mathbf{X}_0^r are initial reference trajectories

```

1: Initialize:
    $\mathbf{X}^r \leftarrow \mathbf{X}_0^r, \mathbf{U}^r \leftarrow \mathbf{U}_0^r, \text{success} \leftarrow \text{false}$ 
2: Compute constraint tightening  $\hat{\mathcal{Y}}_{k+ilk}$  using Algorithm 1 and (15)  $\triangleright \mathbf{U}^r$  and  $\mathbf{X}^r$  used to
   obtain  $K_{k+ilk}$ 
3:  $j = 0$ 
4: while  $j < \text{maxIters}$  do
5:   Obtain new  $\mathbf{U}^r$  and  $\mathbf{X}^r$  by solving Problem 2
6:   Use new  $\mathbf{U}^r$  and  $\mathbf{X}^r$  to update constraint tightening  $\hat{\mathcal{Y}}_{k+ilk}$  using Algorithm 1 and
   (15)
7:   if  $\mathbf{U}^r$  and  $\mathbf{X}^r$  satisfy  $\hat{\mathcal{Y}}_{k+ilk}$  then
8:      $\text{success} \leftarrow \text{true}$ 
9:     break
10:  end if
11:   $j \leftarrow j + 1$ 
12: end while
13: return success,  $\mathbf{U}^r, \mathbf{X}^r$ 

```

Algorithm 3 Robust NMPC

Require: initial reference trajectory \mathbf{Z}_0^r, N, Q, R

```

1:  $\mathbf{Z}^r \leftarrow \mathbf{Z}_0^r$   $\triangleright$  sets current reference trajectory
2: for  $k = 0 \dots N-1$  do
3:   Measure the current state of the system,  $x_k$ 
4:   Run Algorithm 2 to obtain a new valid reference trajectory
5:   if Algorithm 2 returned success then
6:     Update  $\mathbf{Z}^r$  from the new valid reference trajectory returned by Algorithm 2
7:     Apply the control input  $u_{klk} = u_{klk}^r$ 
8:      $k_v \leftarrow k$   $\triangleright$  update time step of last valid solution
9:     Store  $\mathbf{Z}^r$  and  $K_{k+ilk_v}$ , for  $i \in \mathbb{Z}_0^{N-k_v-1}$   $\triangleright$  for use in fallback control input
10:  else
11:    Apply the fallback control input  $u_{klk} = u_{klk_v}^r + K_{klk_v} e_{klk_v}$ .
12:  end if
13: end for

```

Proof. If Assumption 5 is satisfied, then, at time step $k = 0$ a feasible solution is available such that the current output y_k satisfies (2), with input u_{klk}^r being applied to the system. By Algorithm 3, for each future time step $k \in \mathbb{Z}_1^{N-1}$ there are two distinct possibilities.

1. **No success in Algorithm 2:** if Algorithm 2 does not converge to a valid solution at time step k but converged at some $k_v < k$, then the control input $u_k = u_{klk_v}^r + K_{klk_v} e_{klk_v}$ will be applied to the system and Theorem 1 guarantees constraint satisfaction according to (2). The existence of a $k_v < k$ such that a valid reference trajectory is available is guaranteed by Assumption 5.
2. **Success in Algorithm 2:** if Algorithm 2 converges to a valid solution at time step k then the input u_{klk}^r will be applied to the system and by Theorem 1 the current output y_k satisfies (2) and there is a feasible input trajectory for all future time steps such that (2) is satisfied as well.

□

Remark 2. Assuming a valid initial trajectory, as in Assumption 5, is standard in the robust NMPC literature. One way to find a valid initial reference trajectory for the proposed controller is to run Algorithm 2 offline with the initial conditions and replace the objective function in **Problem 2** with a constant, i.e., solving only a feasibility problem and not an optimization problem.

Remark 3. The robust constraint satisfaction guarantees, as provided in Theorems 1 and 2, are sufficient to ensure bounded-input, bounded-output (BIBO) stability. As noted in Koeln et al²¹, for many applications BIBO is not only sufficient but also preferred over asymptotic stability since it allows the controller to use the system dynamics to optimize system operation.

6 | CONSIDERATIONS FOR PRACTICAL IMPLEMENTATION

This section provides details on some of the aspects of the practical implementation of the proposed controller that are relevant to achieve efficient computation. The measures defined here have been adopted to obtain the results shown in Section 7.

6.1 | Set representations and overapproximations

Depending on the set representation and specific algorithms used to compute the Minkowski sum and Pontryagin difference operations in Algorithm 1 and the constraint tightening in **Problem 2**, the underlying numerical computations can be very inefficient. Practical implementations may require trading off accuracy for speed by using overapproximations of some of the computed sets. In this work, sets are represented as zonotopes and sometimes approximated to intervals. Zonotopes are centrally symmetric sets that can be efficiently represented in the so-called G-Rep²² as $\mathcal{Z} = \{c, G\}$, where $c \in \mathbb{R}^n$ is the center of the set and $G = [g_1 \cdots g_{n_g}]$ is a generator matrix whose columns $g_i \in \mathbb{R}^n$ are the generators of the zonotope and n_g is the number of generators. Intervals provide one of the simplest set representations, which allow for very efficient computations although often providing more conservative approximations compared to other representations. An interval of dimension n is a subset of \mathbb{R}^n that can be specified by a lower bound vector \underline{x} and an upper bound vector \bar{x} such that¹⁹

$$\mathcal{I} = [\underline{x}, \bar{x}] = \{x \mid \underline{x}_i \leq x_i \leq \bar{x}_i, \forall i \in \mathbb{Z}_1^n\}.$$

Note that intervals can also be efficiently represented as zonotopes where the generator matrix is simply a diagonal matrix.

The following measures are applied to improve the efficiency of the computations in this work.

- **Zonotope interval hull overapproximation:** as discussed in Section 3, multiple Minkowski sums are required for the computation of the error sets. Since in G-Rep Minkowski sums are executed by concatenating the generator matrices of the operands, with multiple consecutive operations the number of generators of the resulting sets rapidly grows. To keep the set complexity low, zonotopes can be overapproximated by converting them to intervals, which reduces the number of generators to the dimension of the set. This overapproximation of a zonotope is computed by essentially finding the interval hull of the zonotope. Given a zonotope $\mathcal{Z} = \{c, G\}$, its interval hull is given by

$$\text{IH}(\mathcal{Z}) = \left\{ c, \text{diag} \left(\sum_{i=1}^{n_g} |g_i| \right) \right\}.$$

This conversion is applied to the following parts of the control algorithm: after computing each $\mathcal{E}_{k+il|k}$ in Lines 4 and 7 of Algorithm 1, in Line 3 of Algorithm 4, and to the sets involved in the Pontryagin difference operation when computing the sets $\hat{\mathcal{Y}}_{k+il|k}$ in Algorithm 2.

- **Simplified Pontryagin difference:** although performing set operations such as Minkowski additions and linear mappings on zonotopes is very computationally efficient, the same is not true for the exact computation of the Pontryagin difference and it is often necessary to resort to overapproximations²³. However, when performed on intervals where the subtrahend is centered at the origin, the Pontryagin difference operations can be computed exactly and very efficiently. Given two intervals $\mathcal{I}_a = [\underline{x}_a, \bar{x}_a]$ and $\mathcal{I}_b = [-\bar{x}_b, \bar{x}_b]$, with \mathcal{I}_b centered at the origin, their Pontryagin difference can be computed by

$$\mathcal{I}_a \ominus \mathcal{I}_b = [\underline{x}_a + \bar{x}_b, \bar{x}_a - \bar{x}_b].$$

This efficient way of computing the Pontryagin difference is applied when computing the sets $\hat{\mathcal{Y}}_{k+ilk}$ in Algorithm 2. Note that the Pontryagin difference in Algorithm 2 is only used to subtract sets centered at the origin. This is true due to i) disturbance sets \mathcal{D}_k centered at the origin, ii) the fact that every error set \mathcal{E}_{k+ilk} is overapproximated using intervals, and iii) the way the Lagrange remainders are bounded, as shown in Section (6.2), which produces sets centered at the origin.

6.2 | Bounding Lagrange remainders

The i^{th} component of the Lagrange remainder of the Taylor expansion in (5) is given exactly by²⁴

$$\zeta_i(\xi_k) = \frac{1}{2}(z_k - z_k^r)^\top J_i(\xi_k)(z_k - z_k^r),$$

with

$$J_i(\xi_k) = \frac{\partial^2 f_i(\xi_k)}{\partial z^2}.$$

There are multiple methods of bounding linearization errors due to the Lagrange remainder in the Taylor expansion of (1). The CORA toolbox¹⁹ provides functionality to compute $\mathcal{L}(\mathcal{Z}_{k+ilk})$ using different techniques. In this work though, the approach used by Althoff et al²⁴, Section V is applied, which is summarized in Algorithm 4.

Line 1 assumes that the center c of \mathcal{Z}_{k+ilk} coincides with z_{k+ilk}^r , which, considering (13), is true, as long as the sets \mathcal{D}_k have centers at the origin. In Line 4, the max and absolute value operations are performed elementwise and simple interval arithmetic is used to find the maximum absolute values of each component, which is also provided in CORA. In Line 6, the i^{th} component of the Lagrange remainder set is overapproximated by an interval. Finally, in Line 9 all the subintervals are combined to form $\mathcal{L}(\mathcal{Z}_{k+ilk})$.

Algorithm 4 Overapproximation of the Lagrange remainder

Require: $\mathcal{Z}_{k+ilk} = \{c, G\}, G = [g_1 \cdots g_{n_g}]$

```

1:  $\gamma = \sum_{k=1}^{n_g} |g_k|$ 
2: for  $i = 1 \dots n_x$  do
3:    $\mathcal{I}_{\mathcal{Z}} = \text{IH}(\mathcal{Z}_{k+ilk})$ 
4:    $H_i \leftarrow \max(|J_i(z)|), z \in \mathcal{I}_{\mathcal{Z}}$ 
5:    $M_i \leftarrow \frac{1}{2}\gamma^\top H_i \gamma$ 
6:    $\mathcal{L}_i \leftarrow [-M_i, M_i]$ 
7: end for
8:  $\mathcal{L}(\mathcal{Z}_{k+ilk}) = \mathcal{L}_1 \times \cdots \times \mathcal{L}_{n_x}$ 
9: return  $\mathcal{L}(\mathcal{Z}_{k+ilk})$ 
```

7 | NUMERICAL EXPERIMENTS

A series of simulation experiments have been performed to highlight the validity of the proposed approach as well as some of the trade-offs associated with different choices when implementing the proposed controller.

7.1 | Plant model

Simulations have been conducted using an aircraft Fuel Thermal Management System (FTMS) model, depicted in Fig. 1. This model is derived from the simplified model used by Leister and Koeln²⁵ with the ram air cooler replaced by an Air Cycle Machine

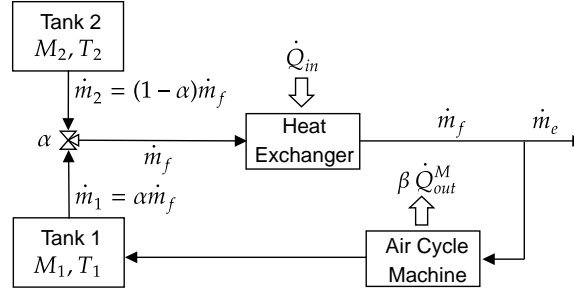


FIGURE 1 Dual-tank FTMS architecture modified with Air Cycle Machine.

(ACM) to provide additional cooling power. The model can be derived from first principles, resulting in the continuous-time dynamics

$$\dot{M}_1 = (1 - \alpha)\dot{m}_f - \dot{m}_e, \quad (17a)$$

$$\dot{M}_2 = -(1 - \alpha)\dot{m}_f, \quad (17b)$$

$$\dot{T}_1 = \frac{(\dot{m}_f - \dot{m}_e)}{M_1} \left[(1 - \alpha)(T_2 - T_1) + \frac{\dot{Q}_{in}}{c_v \dot{m}_f} \right] - \beta \frac{\dot{Q}_{out}^M}{c_v M_1}. \quad (17c)$$

The model states $x = [M_1 \ M_2 \ T_1]^\top$ correspond to the fuel mass in Tanks 1 and 2 and the fuel temperature in Tank 1, respectively. The control inputs $u = [\alpha \ \beta]^\top$ are the split-valve opening and the relative ACM load, respectively. Note that \dot{Q}_{out}^M is the maximum ACM load such that the term $\beta \dot{Q}_{out}^M$ represents the amount of cooling provided by the ACM at any point in time. The only disturbance in the model is \dot{Q}_{h_v} , which is the only time-varying component of the total FTMS heat load \dot{Q}_{in} , which in turn is given by

$$\dot{Q}_{in} = \dot{Q}_F + \dot{Q}_{h_v} + \dot{Q}_{h_e} + (P_p + K_{Q_h} \dot{m}_f). \quad (18)$$

All the other terms in (18) are considered constant. The reader is referred to the work by Leister and Koeln²⁵ for more details on the physical interpretation of the remaining parameters in this model. Table 1 summarizes the values used for each model parameter.

TABLE 1 FTMS MODEL PARAMETERS.

Variable	Description	Units	Nominal Value*	Lower Bound	Upper Bound
M_1	Recirculation tank mass	kg	200	50	2850
M_2	Reservoir tank mass	kg	2850	50	2850
T_1	Recirculation fuel temperature	K	288	250	333
T_2	Reservoir fuel temperature	K	288	-	-
\dot{m}_f	Pumped fuel flow rate	kg/s	1.0	-	-
\dot{m}_e	Engine fuel flow rate	kg/s	0.26	-	-
α	Recirculation fuel fraction	-	-	0	1.0
β	Relative ACM load	-	-	0	1.0
c_v	Fuel specific heat	J/(kg·K)	2,010	-	-
\dot{Q}_F	FADEC heat input	W	1,000	-	-
\dot{Q}_{h_v}	VCS heat input	W	55,000	-	-
\dot{Q}_{h_e}	Engine heat input	W	10,000	-	-
\dot{Q}_{out}^M	Maximum ACM load	W	120,000	-	-
P_p	Fuel pump power	W	50,000	-	-
K_{Q_h}	Fuel pump heat input coeff.	W/kg	-	-	-
			6,618		

*Value also serves as the initial state for M_1 , M_2 , and T_1 .

The discrete-time nonlinear model used in the simulations from this section is obtained by simple forward Euler discretization of the continuous-time dynamics (17).

7.2 | Controller implementations

Since the controller proposed in Algorithm 3 requires the iterative solution of a NLP, that is **Problem 2**, the use of different solvers results in different controller implementations. All simulations were performed in Matlab using CasADi²⁶ to formulate the optimization problems. In this work, three different implementations are compared. The first two use IPOPT²⁷ to solve **Problem 2** and are named IPOPT-MPC1 and IPOPT-MPC2. The difference between both lies in how equation (17c) is entered in the optimization problem formulation. Note that, once the Euler discretization is applied, the equality constraints related to (17c) have bilinear terms on the right-hand side divided by the decision variables related to M_1 . This original formulation is used by IPOPT-MPC2. In IPOPT-MPC1 both sides of these equality constraints are multiplied by the corresponding discretized decision variables related to M_1 . This results in equality constraints that have only bilinear terms on both sides of the equality. As will be seen in the remainder of this section, even though both approaches are mathematically equivalent, the reformulation in IPOPT-MPC1 improves the performance of IPOPT. The third implementation of the controller, SL-MPC, uses a custom NLP solver based on Successive Linearization (SL), very similar to the SL implementation described by Leister and Koeln²⁸ and originally presented by Mao et al²⁹. The reader is referred to the work of Leister and Koeln²⁸ and references therein for more details on the SL algorithm. As with IPOPT-MPC2, the SL-MPC uses the original formulation of the dynamics equations. The SL algorithm internally converts **Problem 2** to a series of Quadratic Programs (QPs) and Gurobi³⁰ is used to solve these QPs. Computations were performed on a desktop computer with a 3.2 GHz i7-8700 processor and 16 GB of RAM.

The initial valid reference trajectory for the controllers is computed offline using the strategy suggested in Remark 2. Also, the following parameters are used to compute the LQR controller matrices: $Q = \text{diag}([1/500 \ 1/100 \ 40/300])$ and $R = \text{diag}([1 \ 0.01])$. The parameter `maxIters` in Algorithm 2 is set to 20 for all controllers. The output vectors here are defined to be simply $y_k = [x_k^\top \ u_k^\top]^\top$ and matrices C_k and D_k are defined accordingly. The output constraints \mathcal{Y}_k are defined as constant intervals matching, for all time steps, the state and input constraints defined in Table 1.

The objective function used in **Problem 2** is

$$\ell(\mathbf{X}_k, \mathbf{U}_k) = \sum_{i=0}^{N-k-1} \Delta u_{k+ik}^\top \Delta u_{k+ik} + w_\beta \beta_{k+ik}^2,$$

where $w_\beta = 5$ is a weighting factor and

$$\Delta u_{k+ik} = (u_{k+ik} - u_{k+i-1k}).$$

For $i = 0$, the term u_{k+i-1k} refers to the input vector at the previous time step. This objective function is designed mainly to incentivize minimum energy use by penalizing the use of the ACM input β and also to encourage smoothness in the control inputs by penalizing the difference between the input vectors at subsequent time steps.

Finally, the controllers implemented here are tested with two different sampling times: $T_s = 50$ seconds and $T_s = 100$ seconds. Since all simulations are performed with a fixed final time of 10,000 seconds, the underlying optimization problems have about twice as many decision variables when $T_s = 50$ seconds. This allows some evaluation of how well these controllers scale with the optimization problem size. However, to allow fair comparisons of the performance of controllers with different sampling times, the following equalized objective function is used

$$\ell_{eq}(\mathbf{X}, \mathbf{U}) = T_s \cdot \ell(\mathbf{X}, \mathbf{U}).$$

This equalized objective function is not implemented in the controllers but is only used for comparisons in Section 7.7. These sampling times are also used to obtain the discrete-time models from the forward Euler discretization of the continuous-time model.

7.3 | Test cases

Recall that the controller formulation in Section 5 considers that the actual disturbance d_k hitting the system has two components: a reference disturbance d_k^r , which can be seen as the predicted disturbance, and an unknown disturbance deviation Δd_k bounded by known sets \mathcal{D}_k . All test cases simulated in this work consider a fixed interval $\mathcal{D}_k = [-27500, +27500]$ W, which is 50% variation over the nominal disturbance variable value, \dot{Q}_{hw} . Also, all test cases consider the same reference trajectory \mathbf{D}_0^r shown in Fig. 2. The test cases consider two specific realizations of Δd_k : Δd_k as a square wave with amplitude given by the extremes of \mathcal{D}_k and Δd_k as a random signal with uniform distribution and maximum amplitude given by \mathcal{D}_k .

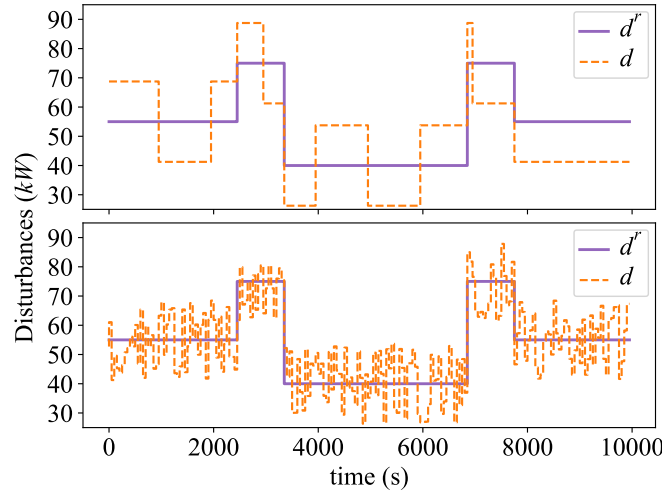


FIGURE 2 Disturbance profiles used in the simulations. Top: Δd_k is a square wave. Bottom: Δd_k is a random signal.

The combination of these disturbance scenarios with the different sampling times mentioned in Section 7.2 results in all test cases evaluated in this work. The specific case when the disturbance from the top of Fig. 2 is applied and $T_s = 100$ seconds will be further referred to as Test Case 1 in order to highlight more detailed results in the remainder of this section.

To illustrate the need for a robust controller in these scenarios, Fig. 3 shows the resulting trajectory when a nominal (non-robust) NMPC controller is applied in closed-loop for Test Case 1. This controller simply solves **Problem 2** once at each time step using IPOPT. However, the tightened constraints $\hat{\mathcal{Y}}_k$ in (16e) are replaced by the original constraints \mathcal{Y}_k , making it effectively a nominal NMPC. As seen in the figure, temperature constraint violations occur as early as $t = 400$ seconds.

7.4 | Error sets and fallback control

Fig. 4 shows an example of the error sets \mathcal{E}_{k+ilk} computed for Test Case 1 at $k = 0$, i.e., based on the initial reference trajectory. Since, as detailed in Section 6, these error sets are approximated by intervals, they are represented in Fig. 4 by their extreme values in each dimension, shown in red. Fig. 4 also shows the actual error e_k obtained for 100 random realizations of Δd_k and with the FTMS system controlled using only the fallback control input (9) based on the same initial reference trajectory used to compute these error sets. This example highlights how the LQR control component in (9) can effectively limit the difference between the reference and actual states as well as how the computed error sets effectively bound these possible error trajectories. Note that two of the error trajectories (in black) actually align with the error set boundaries: these trajectories refer to two additional realizations of Δd_k , namely when the disturbance is constantly at the upper or lower extremes of \mathcal{D}_k respectively. This shows that, specifically for this application example, despite the overapproximations in the computation of the error sets, the sets obtained are not conservative, since there are disturbance realizations that bring the error trajectory very close to the error set boundaries.

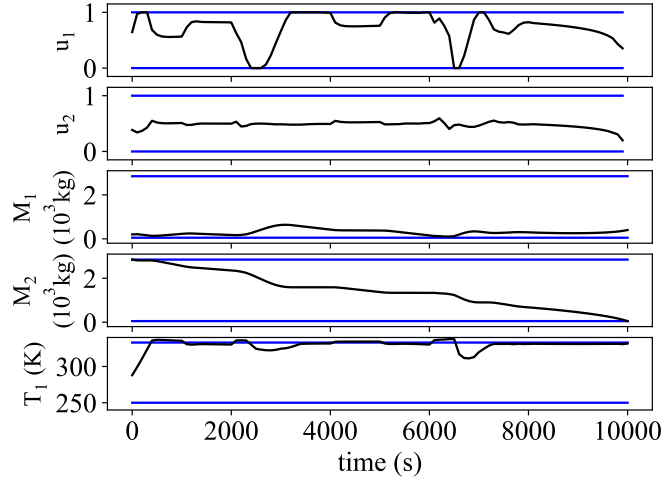


FIGURE 3 State and input trajectories obtained when a nominal NMPC is applied to Test Case 1, with multiple temperature constraint violations. Original constraints are shown in blue.

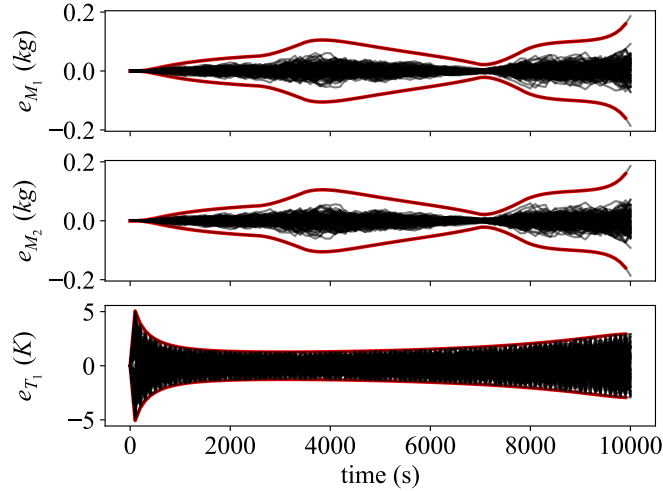


FIGURE 4 Error sets $\mathcal{E}_{k+il|k}$ computed for $k = 0$ (red) and the actual error e_k (black) obtained for 100 random realizations of Δd_k and with the FTMS system controlled using only the fallback control input (9) based on the same reference trajectory used to compute these error sets.

7.4.1 | Effect of the fallback control on closed-loop trajectories and performance

Fig. 5 shows, for Test Case 1 and using IPOPT-MPC1, the effect of the use of the fallback control through three different situations: i) when no fallback control is used, ii) when the fallback control is alternately applied and not applied for periods of 500 seconds, and iii) when only the fallback control is used. It can be seen that, when only the fallback control is used, substantially different trajectories are obtained compared to the case with no fallback control. This highlights the fact that the IPOPT-MPC1 is effectively optimizing the planned trajectory compared to the initial feasible trajectory. In fact, the normalized and equalized objective function values obtained are 1.002 with no fallback control, 1.008 in the alternating case, and 1.520 with fallback control only. Similarly to Fig. 9, the objective function value for IPOPT-MPC2 in Test Case 1 was used for normalization.

The input trajectories for the case when the fallback option is alternately applied highlight one potential effect of using the fallback control: the transitions when going from the fallback to the optimized control option may be considerably abrupt since the newly obtained optimized solution may be quite different from the current fallback option. These transitions can result in

more oscillatory behavior in the state trajectories, although in the present example these are considerably low due to the high damping on the system dynamics. It should be noted that the transitions from the optimized to the fallback control option are in general not abrupt, since at these time steps the fallback control will be based on an optimized trajectory that was obtained just at the previous time step.

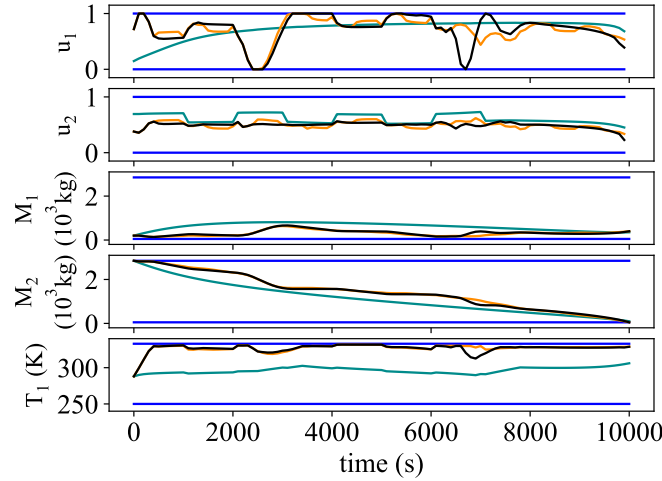


FIGURE 5 State and input trajectories obtained when applying IPOPT-MPC1 (black), IPOPT-MPC1 with the fallback control applied alternately for periods of 500 seconds (orange), and fallback control only (dark green) to Test Case 1. Original constraints are shown in blue.

7.5 | Closed-loop trajectories

Fig. 6 shows the closed-loop state and input trajectories obtained when using each of the three controller implementations for Test Case 1. IPOPT-MPC1 and IPOPT-MPC2 have very similar trajectories since they are essentially using the same solver. The SL-MPC however presents some clear differences in the trajectory obtained, which is explained by the fact that a different solver is being used and each solver may eventually converge to different local minima at the very first time step when **Problem 2** is solved in Algorithm 3, leading to different closed-loop trajectories. It is also clear from Fig. 6 that all three controllers are capable of ensuring robust constraint satisfaction throughout the entire simulation.

To illustrate the amount of spread on the closed-loop trajectories when different realizations of the disturbance are applied, Fig. 7 shows the corresponding trajectories obtained for 100 different random realizations of Δd_k . The trajectories for IPOPT-MPC2 are omitted for conciseness. Interestingly, IPOPT-MPC1 seems to be less consistent in the solutions obtained. Specifically, when observing the behavior of the α input, there is more variation in the input profile compared to the α inputs from SL-MPC. As expected though, robustness is achieved for all simulated realizations of the disturbance for both controllers.

7.6 | Iterations in Algorithm 2

Since the iterations in Algorithm 2 are not guaranteed to converge to a new optimized valid reference trajectory, Fig. 8 gives some insight into the behavior of the three controller implementations in this regard. The figure shows, for each time step in the closed-loop simulations for Test Case 1, how many iterations each controller took to converge to a solution, if converging at all. While IPOPT-MPC2 was able to find valid solutions within the allowed maximum number of iterations IPOPT-MPC1 failed to converge within the maximum number of iterations in two subsequent time steps. The SL-MPC converged to an invalid solution at a few time steps at the beginning of the simulation within just one iteration. This issue stems from the nature of the SL algorithm, where it is possible that the algorithm converges quickly to an infeasible solution. Overall, there is a tendency

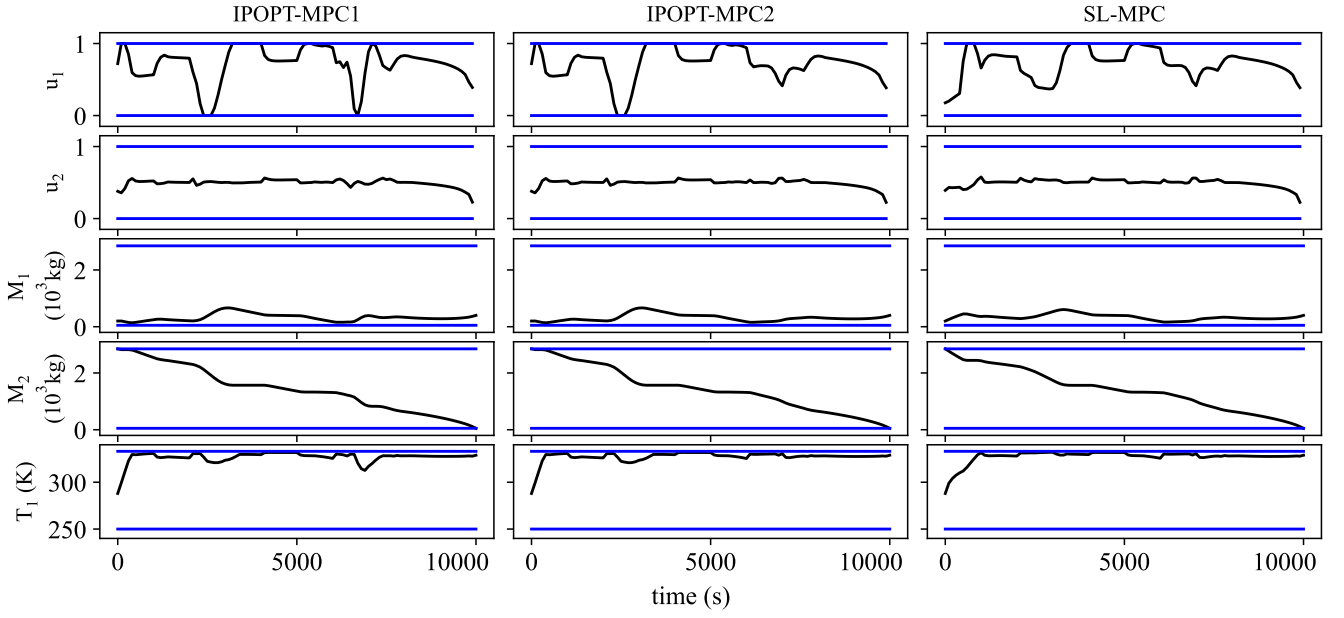


FIGURE 6 State and input trajectories obtained when applying the three robust NMPC controllers to Test Case 1. Original constraints are shown in blue.

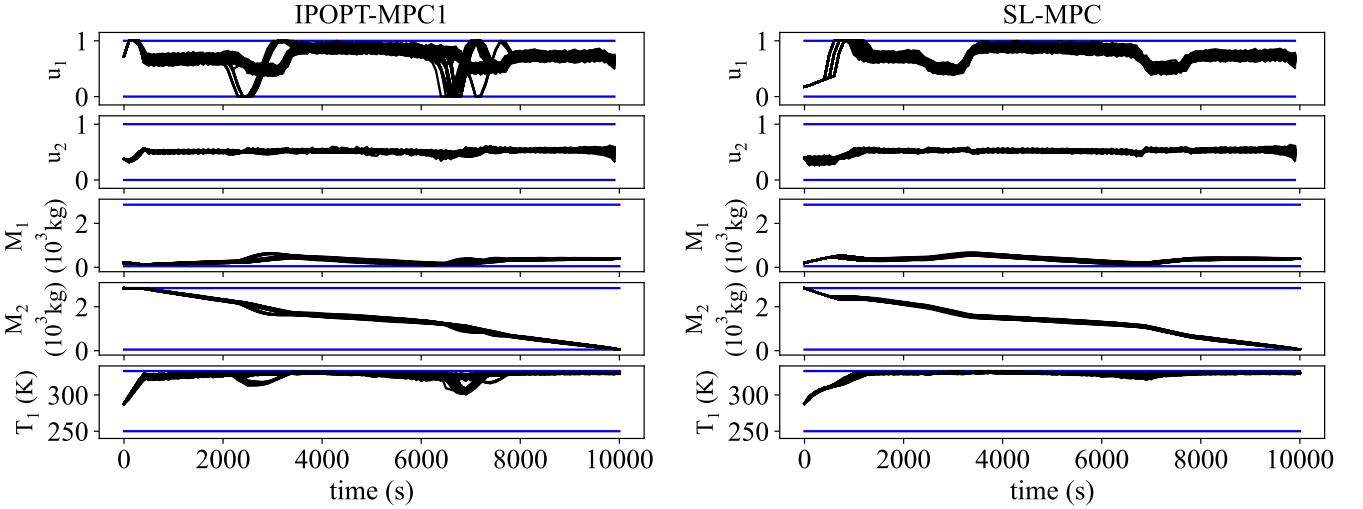


FIGURE 7 State and input trajectories obtained when applying IPOPT-MPC1 and SL-MPC in closed-loop to a 100 different random realizations of Δd_k and with $T_s = 100$. Original constraints are shown in blue.

of the SL-MPC to require slightly fewer iterations to converge compared to the IPOPT-based controllers. This likely helps the SL-MPC use less computation time, as detailed in Section 7.7.

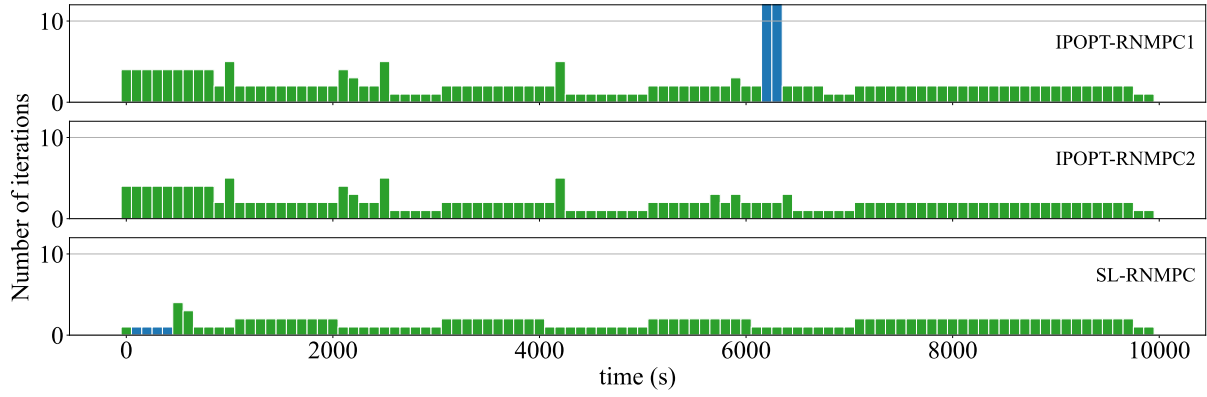


FIGURE 8 Number of iterations taken in Algorithm 2 by each controller for Test Case 1. Time steps when the controllers failed to converge to a valid solution are shown in dark blue.

7.7 | Controller performance

In this section, the performance of the proposed controllers is compared across multiple scenarios as well as with the work of Leeman et al¹³.

7.7.1 | Comparison among implementations of the proposed controller

Figs. 9 to 11 provide a comparison of the performance of all three controllers in terms of equalized objective function values, computed based on the resulting closed-loop trajectories, and computation times. From Fig. 9, it can be seen that the three controllers were able to achieve very similar objective function values.

The similar objective function performance though comes with disparities in computational costs where, in terms of average computation time, the SL-MPC is 15% to 56% faster than IPOPT-MPC1. In terms of the maximum computation time, the results between both controllers are mixed, with a slightly higher value for the SL-MPC at $T_s = 50$ and lower values otherwise. Another difference between the controllers, not shown in the figures, is the fraction of time that the controller spends solving the optimization problem as opposed to computing the constraint tightening for each new iteration: IPOPT-MPC1 spent from 33% to 50% of the time in the solver while SL-MPC spent 16% to 26%.

IPOPT-MPC2 has clearly much higher computation times, both average and maximum, compared to the other two controllers. This stems from the fact that IPOPT-MPC2 is using the original equality constraint formulation in the optimization problem formulation, as discussed in Section 7.2. This formulation not only results in about twice the average computation times compared to IPOPT-MPC1 but also much higher discrepancies in the maximum computation times. These differences between IPOPT-MPC1 and IPOPT-MPC2 highlight one advantage of using SL-MPC: the optimization problem formulations in SL-MPC required no further manipulation of the original nonlinear dynamics function to obtain lower average computation times, as opposed to the manipulations done to implement IPOPT-MPC1.

7.7.2 | Comparison with existing technique¹³

This section provides a comparison of the proposed formulation, specifically the IPOPT-MPC1 implementation, with the controller formulation due to Leeman et al¹³, herein referred to as SLS controller. Similarly to the formulation proposed in this work, SLS controller relies on an LTV approximation of the nonlinear system dynamics. The effect of linearization errors, external disturbances, and parametric uncertainties is encoded into the parameters of the optimization problem and used to tighten the original constraints. Therefore, in their formulation, based on the concept of System Level Synthesis (SLS), both the nominal trajectory as well as the state feedback control law are optimized jointly. This differs from the strategy adopted in this work, where the optimized nominal trajectory and feedback control gains K_{k+ilk} are obtained iteratively in separate steps of Algorithm 2.

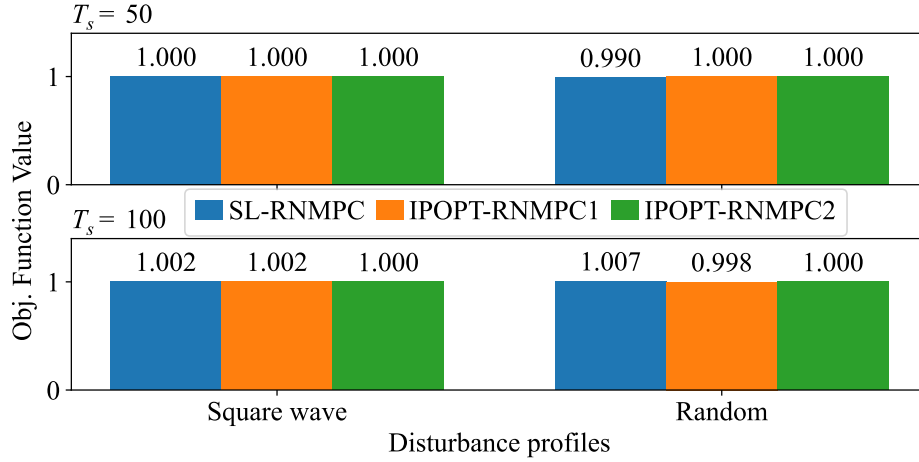


FIGURE 9 Equalized and normalized objective function values obtained for all test cases for the three controllers. The values shown here are normalized by the corresponding values obtained for the IPOPT-MPC2 in each test case.

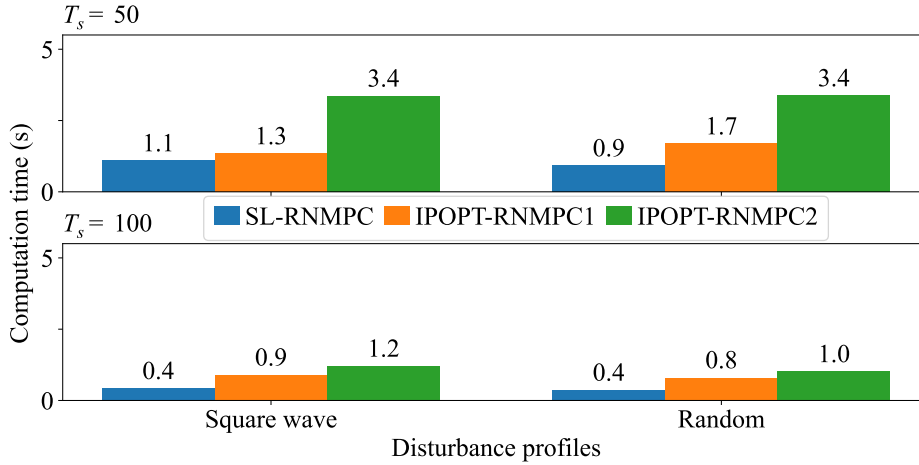


FIGURE 10 Average computation times obtained for all test cases for the three controllers.

In both techniques a key aspect is the size of the reachable sets of the error dynamics, i.e., the LTV system that represents deviations from the nominal optimized trajectory and when controlled with the LTV state-feedback controller. In this work these sets correspond to the \mathcal{E}_{k+ilk} sets for the states and $K_{k+ilk}\mathcal{E}_{k+ilk}$ sets for the inputs. These sets are used for constraint tightening and therefore, the larger the sets the more conservatism is present in the overall solution. The comparison provided here focuses on the solution to the robust optimal control problem for a single time step, particularly in terms of the propagation of the error sets and the corresponding computation times. As a benchmark application example, the satellite post-capture stabilization example provided in Leeman et al¹³ is replicated here. The reader is referred to that reference for more details on this application example. The results for the SLS were obtained through the use of the MATLAB code provided by the authors[†]. The same discrete-time model was used to obtain results for IPOPT-MPC1 with the following exception: Leeman et al¹³ explicitly deal with parametric uncertainties whereas in the implementation for IPOPT-MPC1 such parametric uncertainty was converted into an additional bounded disturbance. The computations with IPOPT-MPC1 were set to provide as much of an accurate comparison with the SLS controller as possible: all model parameters used are the same as described in Leeman et al¹³. The same holds for the

[†] <https://gitlab.ethz.ch/ics/nonlinear-parametric-SLS>

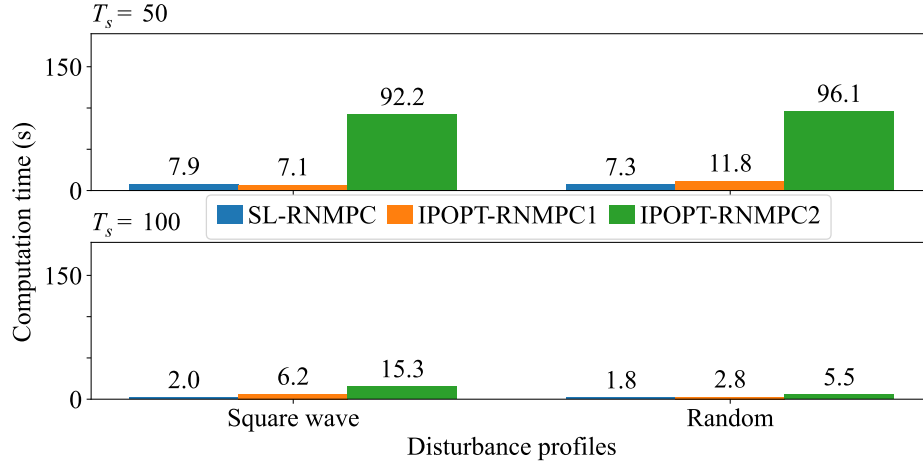


FIGURE 11 Maximum computation times obtained for all test cases for the three controllers.

initial guess and the objective function used. The Q , Q_f , and R matrices of the objective function are also used as the weighting matrices for the LQR controller in IPOPT-MPC1.

Fig. 12 shows the resulting state and input reachable sets of the error dynamics considering a prediction horizon of 5 seconds ($N = 10$) and 10 seconds ($N = 20$). It can be seen, in general, that the reachable sets obtained using IPOPT-MPC1 are smaller, or of about the same size, compared to the sets from the SLS controller. Two exceptions are the input sets for $T = 10$ seconds during the first half of the prediction horizon, where IPOPT-MPC1 is more conservative. Notice that the sets obtained for the first half of the case when $T = 10$ seconds do not need to match the sets for $T = 5$ seconds since different time-varying feedback gains are used for each controller. Also, there are no sets shown for IPOPT-MPC1 for the inputs v_x and v_y at the last time steps because the formulation in this work produces inputs up to time step N while in Leeman et al.¹³ inputs up to time step $N + 1$ are produced. Table 2 shows the computation times for each case. Not only has IPOPT-MPC1 a much lower computation time, about 50 times less for $T = 5$ seconds, but also seems to scale better: doubling the horizon length essentially doubled the computation time for IPOPT-MPC1 but caused a more than 20-fold increase for the SLS controller. The objective function values of each nominal trajectory obtained are also shown in Table 2 to highlight the fact that the use of IPOPT-MPC1 did not cause degraded performance in terms of objective function values. For clarity, the nominal optimized trajectories obtained are not depicted in Fig. 12.

Overall, these results suggest that the proposed formulation has the potential to generate less conservative trajectories, requires much lower computation times, and scales better with the prediction horizon all while providing guarantees of robust constraint satisfaction. These advantages come at the cost of not having guaranteed convergence to an optimal solution, which may require the application of the suboptimal fallback control option. Moreover, the SLS controller has the advantage of providing robust performance guarantees¹³. The results obtained here show that the proposed formulation has promising potential, particularly in applications that have tight computation time requirements or long prediction horizons.

TABLE 2 PERFORMANCE OF THE IPOPT-MPC1 AND THE SLS CONTROLLER.

Controller	$T = 5s$		$T = 10s$	
	Comp. Time (s)	Obj. Func. Value	Comp. Time (s)	Obj. Func. Value
IPOPT-MPC1	1.03	17.29	1.96	17.69
SLS	49.19	21.63	1192.4	21.96

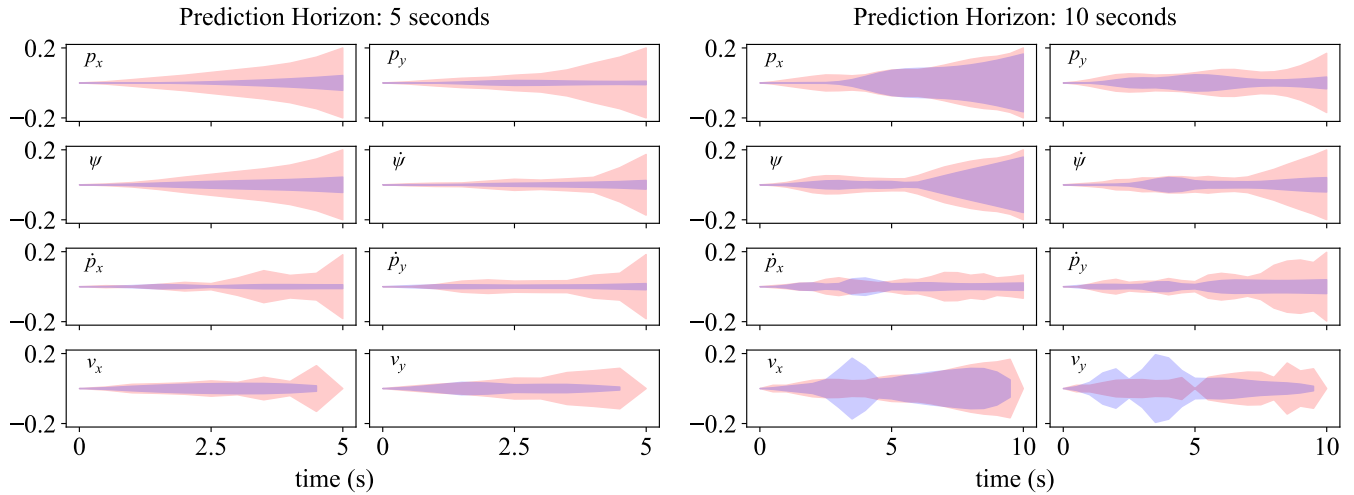


FIGURE 12 Propagation of the reachable sets of the error dynamics for the IPOPT-MPC1 (blue) and SLS (red) controllers for the satellite post-capture stabilization problem¹³ with horizons of 5 and 10 seconds. The reader is referred to Leeman et al¹³ for the meaning of each of the state and input variables shown here.

8 | CONCLUSION

A novel shrinking-horizon robust MPC formulation for nonlinear discrete-time systems was presented. The proposed controller iteratively solves a NLP with tightened constraints to obtain reference trajectories that are used to provide optimized operation with guaranteed robust state and input constraint satisfaction guarantees for all future time steps. When the iterations fail to produce a valid reference trajectory, a suboptimal fallback control option is used that preserves the guaranteed constraint satisfaction. The proposed controller was tested, with three different NLP solvers, using an aircraft FTMS model under different disturbance scenarios. All three controller implementations provided robust optimized system operation with overall less computational load from the controller based on a Successive Linearization solver when compared to the controllers that use IPOPT to solve the underlying NLP. A comparison with one of the existing techniques in the literature showed promising results in terms of conservatism, computation time, and scalability. Future work will focus on extending the proposed robust controller formulation to the receding-horizon case.

ACKNOWLEDGMENTS

This material is based upon work supported by the Office of Naval Research under award number N00014-22-1-2247. Any opinions, findings, and conclusions or recommendations expressed in this material are those of the authors and do not necessarily reflect the views of the Office of Naval Research.

REFERENCES

1. Limon Marruedo D, Alamo T, Camacho E. Stability analysis of systems with bounded additive uncertainties based on invariant sets: Stability and feasibility of MPC. In: . 1. Proceedings of the American Control Conference. 2002:364-369 vol.1
2. Richards A. Robust Model Predictive Control for Time-Varying Systems. In: Proceedings of the 44th IEEE Conference on Decision and Control. 2005:3747-3752
3. Mayne D, Seron M, Raković S. Robust model predictive control of constrained linear systems with bounded disturbances. *Automatica*. 2005;41(2):219-224. doi: <https://doi.org/10.1016/j.automatica.2004.08.019>
4. Bravo JM, Alamo T, Camacho EF. Robust MPC of Constrained Discrete-Time Nonlinear Systems Based on Approximated Reachable Sets. *Automatica*. 2006;42(10):1745-1751. doi: [10.1016/j.automatica.2006.05.003](https://doi.org/10.1016/j.automatica.2006.05.003)
5. Pin G, Raimondo DM, Magni L, Parisini T. Robust Model Predictive Control of Nonlinear Systems With Bounded and State-Dependent Uncertainties. *IEEE Transactions on Automatic Control*. 2009;54(7):1681-1687. doi: [10.1109/TAC.2009.2020641](https://doi.org/10.1109/TAC.2009.2020641)
6. Cannon M, Buerger J, Kouvaritakis B, Rakovic S. Robust Tubes in Nonlinear Model Predictive Control. *IEEE Transactions on Automatic Control*. 2011;56(8):1942-1947. doi: [10.1109/TAC.2011.2135190](https://doi.org/10.1109/TAC.2011.2135190)
7. Mayne DQ, Kerrigan EC, van Wyk EJ, Falugi P. Tube-Based Robust Nonlinear Model Predictive Control. *International Journal of Robust and Nonlinear Control*. 2011;21(11):1341-1353. doi: [10.1002/rnc.1758](https://doi.org/10.1002/rnc.1758)

8. Zhao M, Can-Chen J, Ming-Hong S. Robust Contractive Economic MPC for Nonlinear Systems with Additive Disturbance. *International Journal of Control, Automation, and Systems: IJCAS*. 2018;16(5):2253–2263. doi: 10.1007/s12555-017-0669-y
9. Köhler J, Soloperto R, Müller MA, Allgöwer F. A Computationally Efficient Robust Model Predictive Control Framework for Uncertain Nonlinear Systems. *IEEE Transactions on Automatic Control*. 2021;66(2):794–801. doi: 10.1109/TAC.2020.2982585
10. Morato MM, Cunha VM, Santos TLM, Normey-Rico JE, Sename O. Robust Nonlinear Predictive Control through qLPV Embedding and Zonotope Uncertainty Propagation. *IFAC-PapersOnLine*. 2021;54(8):33–38. doi: 10.1016/j.ifacol.2021.08.577
11. Messerer F, Diehl M. An Efficient Algorithm for Tube-based Robust Nonlinear Optimal Control with Optimal Linear Feedback. In: IEEE 60th Conference on Decision and Control (CDC). 2021:6714–6721
12. Doff-Sotta M, Cannon M. Difference of Convex Functions in Robust Tube Nonlinear MPC. In: IEEE 61st Conference on Decision and Control (CDC). 2022:3044–3050
13. Leeman AP, Sieber J, Bennani S, Zeilinger MN. Robust Optimal Control for Nonlinear Systems with Parametric Uncertainties via System Level Synthesis. Preprint posted online: arXiv:2304.00752; 2023.
14. Kim T, Elango P, Acikmese B. Joint Synthesis of Trajectory and Controlled Invariant Funnel for Discrete-time Systems with Locally Lipschitz Nonlinearities. Preprint posted online: arXiv:2209.03535; 2024.
15. Murillo M, Sánchez G, Giovanini L. Iterated Non-Linear Model Predictive Control Based on Tubes and Contractive Constraints. *ISA Transactions*. 2016;62:120–128. doi: 10.1016/j.isatra.2016.01.008
16. Leeman AP, Köhler J, Messerer F, Lahr A, Diehl M, Zeilinger MN. Fast System Level Synthesis: Robust Model Predictive Control using Riccati Recursions. Preprint posted online: arXiv:2401.13762; 2024.
17. Doman DB. Fuel Flow Topology and Control for Extending Aircraft Thermal Endurance. *Journal of Thermophysics and Heat Transfer*. 2018;32(1):35–50. doi: 10.2514/1.T5142
18. Koeln JP, Alleyne AG. Two-Level Hierarchical Mission-Based Model Predictive Control. In: Annual American Control Conference (ACC). 2018:2332–2337
19. Althoff M, Kochdumper N, Wetzlinger M. CORA 2022 Manual. Accessed September 11, 2023. <https://tumcps.github.io/CORA; 2022>.
20. Castro JES, Hashimoto RF, Barrera J. Analytical Solutions for the Minkowski Addition Equation. In: Lecture Notes in Computer Science. Mathematical Morphology and Its Applications to Signal and Image Processing. Springer 2013:61–72
21. Koeln J, Raghuraman V, Hencsey B. Vertical hierarchical MPC for constrained linear systems. *Automatica*. 2020;113:108817. doi: <https://doi.org/10.1016/j.automatica.2020.108817>
22. McMullen P. On Zonotopes. *Transactions of the American Mathematical Society*. 1971;159(0):91–109. doi: 10.1090/S0002-9947-1971-0279689-2
23. Yang L, Zhang H, Jeannin JB, Ozay N. Efficient Backward Reachability Using the Minkowski Difference of Constrained Zonotopes. *IEEE Transactions on Computer-Aided Design of Integrated Circuits and Systems*. 2022;41(11):3969–3980. doi: 10.1109/TCAD.2022.3197971
24. Althoff M, Stursberg O, Buss M. Reachability Analysis of Nonlinear Systems with Uncertain Parameters Using Conservative Linearization. In: 47th IEEE Conference on Decision and Control. 2008:4042–4048
25. Leister DD, Koeln JP. Nonlinear Hierarchical MPC for Maximizing Aircraft Thermal Endurance. In: ASME Dynamic Systems and Control Conference. 2020
26. Andersson JAE, Gillis J, Horn G, Rawlings JB, Diehl M. CasADi: A Software Framework for Nonlinear Optimization and Optimal Control. *Mathematical Programming Computation*. 2019;11(1):1–36. doi: 10.1007/s12532-018-0139-4
27. Byrd RH, Hribar ME, Nocedal J. An Interior Point Algorithm for Large-Scale Nonlinear Programming. *SIAM Journal on Optimization*. 1999;9(4):877–900. doi: 10.1137/S1052623497325107
28. Leister DD, Koeln JP. Nonlinear Hierarchical MPC With Application to Aircraft Fuel Thermal Management Systems. *IEEE Transactions on Control Systems Technology*. 2023:1–14. doi: 10.1109/TCST.2022.3214730
29. Mao Y, Szmuk M, Açikmeşe B. Successive Convexification of Non-Convex Optimal Control Problems and Its Convergence Properties. In: IEEE 55th Conference on Decision and Control (CDC). 2016:3636–3641
30. Gurobi Optimization, LLC. Gurobi Optimizer Reference Manual. Accessed September 11, 2023. <https://www.gurobi.com; 2021>.

□

APPENDIX

A LQR CONTROLLER

The following equations can be used to derive a LTV LQR controller for a LTV system with dynamics matrices A_k and B_k using a dynamic programming approach. The Q and R matrices are tunable parameters. The K_{k+ilk} gains are to be computed backwards in time as

$$\begin{aligned}
 P_{k+N|k} &= Q, \\
 P_{k+ilk} &= Q + A_{k+i}^T P_{k+i+1|k} A_{k+i} - A_{k+i}^T P_{k+i+1|k} B_{k+i} (R + B_{k+i}^T P_{k+i+1|k} B_{k+i})^{-1} B_{k+i}^T P_{k+i+1|k} A_{k+i}, \\
 K_{k+ilk} &= (R + B_{k+i}^T P_{k+i+1|k} B_{k+i})^{-1} B_{k+i}^T P_{k+i+1|k} A_{k+i}.
 \end{aligned}$$